Available online at www.sciencedirect.com

SCIENCE DIRECT®

Nuclear Medicine and Biology 33 (2006) 227–237

NUCLEAR MEDICINE — AND — BIOLOGY

www.elsevier.com/locate/nucmedbio

In vitro and in vivo investigation of matrix metalloproteinase expression in metastatic tumor models

Jennifer E. Sprague[1], Wen Ping Li[1], Kexian Liang, Samuel Achilefu, Carolyn J. Anderson*

Mallinckrodt Institute of Radiology, Washington University School of Medicine, St. Louis, MO 63110, USA

Received 31 March 2005; received in revised form 17 October 2005; accepted 20 October 2005

Abstract

Introduction: Overexpression of matrix metalloproteinases (MMPs), particularly MMP-2 and MMP-9, has been correlated with poor prognosis in several cancer types including lung, colon and breast. Noninvasive detection of MMP expression might allow physicians to better determine when more aggressive cancer therapy is appropriate. The peptide CTT (CTTHWGFTLC) was identified as a selective inhibitor of MMP-2/9 that inhibits the growth of MDA-MB-435 human breast cancer xenografts.

Methods: CTT was conjugated with the bifunctional chelator DOTA (1,4,7,10-tetraazacyclotetradecane-*N*,*N*′,*N*″,*N*‴-tetraacetic acid) for radiolabeling with ^{64}Cu ($t_{1/2}$=12.7 h, 17.4% β^+, 39% β^-), a radionuclide suitable for positron emission tomography (PET). In vitro affinity was determined in a fluorogenic substrate assay. Tumor gelatinase targeting was evaluated in both biodistribution and microPET imaging studies.

Results: Cu(II)-DOTA-CTT inhibited hMMP-2 (EC_{50}=8.7 μM) and mMMP-9 (EC_{50}=18.2 μM) with similar affinity to CTT (hMMP-2 EC_{50}=13.2 μM; mMMP-9 EC_{50}=11.0 μM). In biodistribution and microPET imaging studies, ^{64}Cu-DOTA-CTT was taken up by MMP-2/9-positive B16F10 murine melanoma tumors. Subsequently, imaging studies using ^{64}Cu-DOTA-CTT were performed on MDA-MB-435 tumor-bearing mice. With zymography, tumor MMP-2/9 expression in this model was shown to be inconsistent, resulting in microPET detection of the MDA-MB-435 tumor in only 1 of 24 imaged mice. Following limited imaging success, ^{64}Cu-DOTA-CTT was shown to have poor in vivo stability.

Conclusions: Despite some evidence for selective uptake of ^{64}Cu-DOTA-CTT by gelatinase-expressing tumors, the low affinity for MMP-2 and MMP-9 and in vivo instability make this an inadequate radioligand for in vivo tumor evaluation.

Keywords: PET imaging; Cancer; MMP

1. Introduction

Tumor invasion and metastasis define malignancy and are the major causes of cancer mortality. Metastasis is a complex multi-step process involving detachment of tumor cells from the primary tumor, invasion through the basement membrane, intravasation into the circulatory system, extravasation at a distant site and outgrowth of a secondary tumor [1]. Growth beyond 1 to 2 mm diameter of both primary and metastatic tumors requires neoangiogenesis to supply the tumor with nutrients [2]. Matrix metalloproteinases (MMPs), a family of Zn^{2+}-dependent endopeptidases, particularly 72-kDa (MMP-2) and 92-kDa (MMP-9) gelatinases, play important roles in these processes [3–9].

The overproduction and unrestrained activity of MMPs have been linked to malignancy in a variety of tumors including brain, colon, lung, bladder, melanoma and breast.

Abbreviations: % ID, percent injected dose; ACN, acetonitrile; APMA, 4-aminophenylmercuric acetate; CTT, CTTHWGFTLC; DIEA, diisopropyl ethylamine; DMF, dimethyl formamide; DOTA, 1,4,7,10-tetraazacyclododecane-*N*,*N*′,*N*″,*N*‴-tetraacetic acid; CB-TE2A, 4,11-bis(carboxymethyl)-1,4,8,11-tetraazabicyclo[6.6.2]hexadecane; EC_{50}, 50% effective concentration; ECM, extracellular matrix; ES-MS, electrospray mass spectrometry; Fmoc, fluorenylmethyl; HBTU, 2-(1*H*-benzotriazol-1-yl)-1,1,3,3-tetramethyluronium hexafluoro phosphate; HOBt, *N*-hydroxybenzotriazole; HPLC, high-performance liquid chromatography; HWGF, His-Trp-Gly-Phe; IC_{50}, 50% inhibitory concentration; mAb, monoclonal antibody; MeOH, methanol; MMP, matrix metalloproteinase; OSEM, ordered subsets expectation maximization; PET, positron emission tomography; ROI, region of interest; SDS, sodium dodecyl sulfate; SPECT, single photon emission tomography; STT, STTGHFWTLS; SUV, standard uptake value; TETA, 1,4,8,11-tetraazacyclotetradecane-1,4,8,11-tetraacetic acid; TFA, trifluoroacetic acid; TLC, thin layer chromatography.

* Corresponding author. Tel.: +1 314 362 8427; fax: +1 314 362 9940.
E-mail address: andersoncj@wustl.edu (C.J. Anderson).

[1] These two authors contributed equally to this research.

0969-8051/$ – see front matter © 2006 Elsevier Inc. All rights reserved.
doi:10.1016/j.nucmedbio.2005.10.011

A negative association between elevated MMP expression and prognosis has been well documented with the metastatic phenotype of carcinomas, especially breast cancer [10]. For example, lack of MMP-2 expression has been associated with improved survival in women with estrogen receptor negative breast cancers, otherwise considered poor prognosis [11]. Other studies have associated MMP-2 and/or MMP-9 expression with increased nodal metastasis and poor prognosis in breast cancer [12,13].

Imaging gelatinase expression in tumors using positron emission tomography (PET), single photon emission tomography (SPECT) or near-infrared fluorescence may provide a noninvasive means to predict the metastatic potential of a tumor. Indeed, there has been a growing interest in the use of MMP inhibitors as radiotracers to image tumors that overexpress MMPs [14–16]. Several synthetic sulfonamide-based MMP inhibitors have been radiolabeled with carbon-11, fluorine-18 or iodine-123, and preliminary evaluations of these radiotracers for tumor imaging have been performed. However, selective binding of labeled compounds to specific MMPs was not demonstrated, and high nonspecific binding was observed in vivo [17–19].

The cyclic decapeptide CTT**HWGF**TLC (CTT), containing a His-Trp-Gly-Phe (HWGF) motif, indicated in bold, has been described as a selective MMP-2 and MMP-9 inhibitor that reduced the migration of both human endothelial and tumor cells, and prevented tumor growth and invasion in animal models [20]. Kuhnast et al. [21] recently reported derivatization and radiolabeling CTT with ^{125}I for in vitro and in vivo studies. Unimpaired inhibition of MMP-2 activity was demonstrated in vitro for the derivatized CTT, and the iodinated peptide showed no degradation by activated MMP-2 and MMP-9. However, poor in vivo stability of the ^{125}I-D-Tyr-modified peptide resulted in low tumor uptake. More recently, Medina et al. reported selective imaging of MMP-2 in tumors using liposomes radiolabeled with ^{99m}Tc-CTT [22].

Here, a PET-compatible approach for selective molecular imaging of gelatinases was used; CTT was conjugated to the chelator DOTA (1,4,7,10-tetraazacyclotetradecane-*N*,*N*′,*N*″,*N*‴-tetraacetic acid) (Fig. 1) for radiolabeling with ^{64}Cu. Copper-64 ($t_{1/2}$=12.7 h) is both a positron (β^+) (17.4%, $E_{\beta+max}$=656 keV) and beta minus (β^-) emitter (39%, $E_{\beta-max}$=573 keV) that is readily produced in high specific activity on a small biomedical cyclotron at Washington University [23]. The decay characteristics of ^{64}Cu make it suitable for PET imaging as well as radiotherapy when targeted to tumors using monoclonal antibodies (mAb) or peptides [24–26].

The inhibitory activity of Cu(II)-DOTA-CTT against MMP-2 and MMP-9, and the serum stability were evaluated in vitro. The linear scrambled peptide DOTA-STT**GHFW**TLS (STT) was used as a negative control since linearization had previously been reported to reduce MMP-2 inhibitory activity 10-fold [20]. Biodistribution and microPET studies were carried out in B16F10 murine melanoma-bearing mice. In addition, microPET imaging with ^{64}Cu-DOTA-CTT was used to investigate gelatinase expression at various time points postimplantation of MDA-MB-435 human breast cancer in mice.

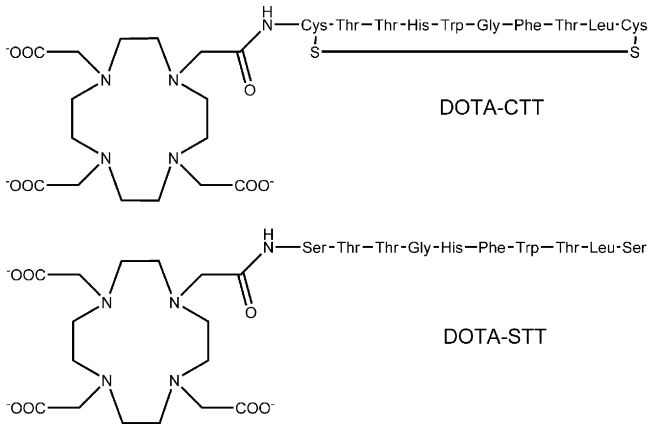

Fig. 1. Structure of DOTA-CTT and DOTA-STT.

2. Materials and methods

2.1. Reagents and analyses

All chemicals were obtained from commercial sources and used without further purification. Copper-64 was produced on a biomedical cyclotron CS-15 at Washington University School of Medicine, using the previously reported method [27]. Sources of other reagents were as follows: proMMP-2 and proMMP-9 enzymes, Chemicon (Temecula, CA); Ilomastat, CTT and fluorogenic substrates (MMP substrate III, fluorogenic or MMP-1/MMP-9 substrate), Calbiochem (San Diego, CA); rat serum and gelatin, Sigma-Aldrich (St. Louis, MO); prestained molecular weight color standard and Coomassie blue R-250, Bio-Rad (Richmond, CA); Waters C18 silica gel plates (KC18F), Fisher Scientific (Pittsburgh, PA); copper (II) chloride ($CuCl_2$), Johnson Matthey (West Deptford, New Jersey); trifluoroacetic acid (TFA), J.T. Baker (Chicago, IL); DOTA-tris(*t*-butyl ester), Macrocyclics (Dallas, TX); Fmoc-protected amino acids, Novabiochem (San Diego, CA). All other chemicals were purchased from Sigma-Aldrich.

Radio-TLC was carried out by using a 7:3 MeOH/10% ammonium acetate mobile phase on C-18 plates and a Bioscan 200 imaging scanner (Bioscan, Washington, DC). Analytical reversed-phase HPLC was accomplished on a Waters (Milford, MA) 600E chromatography system with a Waters 991 photodiode array detector and an Ortec Model 661 (EG&G Instruments, Oak Ridge, TN) radioactive detector. Samples (^{64}Cu-DOTA-CTT and ^{64}Cu-DOTA-STT) were analyzed on a Vydac Protein & Peptide C-18 column (2.2×10 cm). The mobile phase was H_2O (0.1% TFA) (solvent A) and 90% acetonitrile (ACN) (0.1% TFA) (solvent B). The gradient consisted of 5% B to 75% B in 15 min (1.0 ml/min flow rate). Metabolic samples were analyzed by size-exclusion HPLC on a Superose 12 HR

10/300 column (Amersham Biosciences, Uppsala, Sweden) eluted with 20 mM HEPES, 150 mM NaCl, pH 7.3 as mobile phase. Millenium 32 software (Waters) was used to quantify chromatograms by integration. Radioactive samples were counted using a Beckman 8000 automated well-typed gamma counter (Fullerton, CA). ES-MS was accomplished using a Waters Micromass ZQ.

2.2. Synthesis of DOTA-CTT

The initial batch of DOTA-CTT was prepared on an ACT APEX 396 peptide synthesizer by standard fluorenylmethyl (Fmoc) protocol [28], as described previously [29,30]. Briefly, a Rink amide resin preloaded with Fmoc-Cys (Acm)-OH on a 25-μmol scale was placed in a reaction vessel. Subsequent Fmoc-protected amino acids (75 μmol) were sequentially coupled to the resin-bound amino acid from the carboxyl to amino terminus. Fmoc removal was accomplished with 20% piperidine in dimethyl formamide (DMF). The coupling reagents *N*-hydroxybenzotriazole (HOBt, 75 μmol) and 2-(1*H*-benzotriazol-1-yl)-1,1,3,3-tetramethyluronium hexafluoro phosphate (HBTU, 75μmol) were used for the peptide assembly in the presence of DIEA (150 μmol). Intramolecular disulfide cyclization was accomplished by removing the peptide resin from the synthesizer and adding it to a 2-ml solution of thalium trifluoroacetate (23 mg) in DMF. The mixture was gently swirled on an agitator for 1.5 h and filtered. The resulting peptide resin was washed sequentially with DMF/H_2O (1:1), DMF, methanol and dichloromethane. The resin was returned to the synthesizer, and the N-terminal Fmoc protecting group was removed with piperidine, as described above. Coupling of the orthogonally protected tri-*t*-butyl-DOTA (75 μmol) was performed with HBTU/HOBt. Peptide cleavage from the resin and concomitant removal of the amino acid side-chain protecting groups were accomplished by adding a cleavage mixture (1 ml) of TFA (85%), distilled water (5%), phenol (5%) and thioanisole (5%) to the resin and gently mixing the content for 3 h. The crude peptide was precipitated in cold *t*-butyl methyl ether and lyophilized in acetonitrile/water (2:3) mixture. The resulting powder was purified by HPLC to give 3 mg (8% yield) of the desired compound. HPLC purity was >95%.

STT, DOTA-STT and additional DOTA-CTT were synthesized by CS Bio (San Carlos, CA). DOTA-STT was 96% pure by HPLC. The identity was confirmed by ES-MS "*m/z* $(M+H)^+$=1522.47, calcd=1522.66." DOTA-CTT was shown to be 95% pure by HPLC, and the identity was confirmed by ES-MS *m/z* $(M+H)^+$=1552.27, calcd=1552.80.

2.3. Radiolabeling with $^{64}Cu^{2+}$ and complexation with $^{nat}Cu^{2+}$

Radiolabeling of DOTA-CTT and DOTA-STT with ^{64}Cu was carried out by incubating 1–5 μg of the conjugate with 1–5 mCi (37–185 MBq) of ^{64}Cu in 0.1 M ammonium acetate (pH 6.5) for 30 min at room temperature [31] or at 70°C. Radiochemical purity of ^{64}Cu-DOTA-CTT was determined by radio-TLC and was confirmed by radio-HPLC. ^{nat}Cu(II)-DOTA-CTT was prepared using the same method at 1 mM final concentration. Formation of ^{nat}Cu(II)-DOTA-CTT was confirmed by ES-MS [*m/z* for $C_{68}H_{95}N_{17}O_{21}S_2Cu$ $(M+H)^+$=1613.12; calcd 1613.57].

2.4. Inhibition studies

Inhibitory activity of the synthetic peptides was determined using a quenched fluorogenic substrate [32–34]. Briefly, proMMPs were activated by reaction with 4-aminophenylmercuric acetate (0.05 mM APMA, 0.05 M borate buffer, 0.01 mM $ZnCl_2$, 5 mM $CaCl_2$) at 37°C for 30 min (proMMP-9) or 1 h (proMMP-2). The activation reaction was quenched by 10-fold dilution in assay buffer (50 mM Tris, pH 7.6, 50 mM NaCl, 10 mM $CaCl_2$, 0.05% Brij-35). Activated MMPs (0.5 nM final concentration) were mixed with the inhibitor [CTT, STT, Cu(II)-DOTA-CTT or Cu(II)-DOTA-STT] in assay buffer in a black 96-well plate (Greiner) and incubated 2 h at 37°C. Ilomastat, a broad-spectrum MMP inhibitor, was used as a positive control [35]. Fluorogenic substrate (MMP substrate III, fluorogenic or MMP-1/MMP-9 substrate) (10 μM final concentration) was added, and the reaction was allowed to proceed at 37°C (3 h for MMP-9, 8 h for MMP-2). Fluorescence intensity due to substrate cleavage was measured at 360 nm excitation/465 nm emission using a Perkin-Elmer HTS 7000 Bio Assay Reader (Norwalk, CT). Triplicate measurements were averaged to obtain each data point. Fluorescence was normalized to % control activity. Activity plots were analyzed using GraphPad Prism 4.0 (San Diego, CA). EC_{50} values represent the mean of at least two experiments unless otherwise noted.

2.5. Serum stability

The stability of radiolabeled DOTA-CTT and DOTA-STT was evaluated in vitro in rat serum (Sigma-Aldrich). Briefly, 50 μl radiolabeled peptide (500 μCi, 0.5 μg) was incubated with 500 μl of rat serum at 37°C. Aliquots (1 μl) were removed at various time points (0.5, 1, 2, 4, 6, 24 h postmixing) and analyzed by radio-TLC and RP-HPLC as described above. The percentage of radioactivity in the complex form was determined.

2.6. Animal models

All animal experiments were performed in compliance with the Guidelines for the Care and Use of Research Animals established by Washington University's Animal Studies Committee. B16F10 cells were obtained from Katherine N. Weilbaecher, MD (Washington University, St. Louis) [36], and MDA-MB-435 cells were obtained from Janet E. Price, PhD (MD Anderson Cancer Center, Houston, TX) [37]. The B16F10 murine melanoma model was established in male C57BL/6 mice (Charles River Laboratories, Wilmington, MA) by subcutaneously injecting 5×10^5 cells/100 μl per mouse at 8–10 weeks of age. The

MDA-MB-435 human breast cancer model was established in 8- to 10-week-old, female *nu*/*nu* mice (Charles River Laboratories) by injecting 10^5 cells/100 μl in the right mammary fat pad.

2.7. Biodistribution

Biodistribution studies were carried out in both C57BL/6 normal and B16F10 tumor-bearing mice (13 days post-implantation). Mice were injected via the tail vein with ^{64}Cu-DOTA-CTT (10 μCi, 0.08 μg) or ^{64}Cu-DOTA-STT (10 μCi, 0.08 μg) in 100 μl of isotonic saline ($n=5$ mice/time point). At 1, 2 and 24 h postinjection, mice were anesthetized with 1–2% isoflurane and sacrificed by cervical dislocation; organs of interest (blood, tumor, muscle, lung, spleen, kidney, liver, small intestine) were removed and weighed. Subsequently, the activity in tissues and injection standards was measured in a gamma counter. Samples were corrected for radioactive decay to calculate the percent injected-dose per gram (% ID/g) of tissue and percent injected-dose per organ (% ID/organ) by comparison with a standard representing the injected dose.

2.8. MicroPET imaging of B16F10 tumor-bearing mice

Positron emission tomography (PET) imaging was performed using a microPET-R4 scanner (Concorde Microsystems, Knoxville, TN). The microPET-R4 (Concorde Microsystems) is the first commercially available small animal PET scanner. Its design is based on the UCLA prototype [38]. The microPET-R4 contains four rings of 24 lutetium oxyorthosilicate crystal block (2×2×1 cm) detectors; each crystal block is subdivided into an 8×8 matrix. The transaxial field of view (FOV) is 10.8 cm, the axial FOV is 7.8 cm. The reconstructed image resolution is 2.3 mm full width at half maximum (FWHM) close to the center of the FOV. A complete performance evaluation of the scanner is found in Knoess et al. [39]. Imaging studies were carried out on eight mice bearing B16F10 tumors (12 days postimplantation). Mice were administered 200 μCi (~0.2 μg) of ^{64}Cu-DOTA-CTT or ^{64}Cu-DOTA-STT via tail vein injection. At 1, 4 and 24 h postinjection, mice were anesthetized with 1–2% isoflurane, positioned supine, immobilized and imaged. Two mice were scanned side by side; one mouse was given a dose of ^{64}Cu-DOTA-CTT, and the other one received ^{64}Cu-DOTA-STT. Scan time was 10 min. Images were reconstructed using ordered subsets expectation maximization (OSEM); no attenuation correction was used. Post-PET biodistribution was performed, and tumors, blood and liver were kept on ice before and after counting.

For quantitative analysis, regions of interest (ROIs) on microPET images were drawn by a single individual to minimize variation in region selection. Regions of interest for tumor, liver and kidneys were drawn to encompass the entire organ in the transaxial plane (three slices). Standard uptake values (SUVs) ([nCi/cc]*[weight (g)/injected dose (nCi)]) were generated by measuring ^{64}Cu activity in each ROI.

2.9. MicroPET imaging of MDA-MB-435 tumor-bearing mice

Mice bearing palpable MDA-MB-435 tumors were administered 100–200 μCi ^{64}Cu-DOTA-CTT (0.1 mCi/μg peptide) via tail vein injection at various times post-tumor implantation (5–13 weeks). At 1, 2 and 4 h postinjection, mice were microPET imaged as described above. Immediately after the last imaging time point, each mouse was sacrificed, and a biodistribution was performed as described above. Tumors were dissected free of surrounding tissue (muscle and fat) and kept on ice before and after counting.

2.10. Gelatin zymography

Tissue extracts for gelatin zymography were prepared immediately upon sacrifice, or tumors were flash frozen in liquid nitrogen and stored at −80°C until extracts were prepared as previously described [40]. Briefly, fragments of tumor tissue were suspended in 0.1 M Tris–HCl buffer, pH 7.8, with 0.15 M NaCl, 10 mM $CaCl_2$ and 0.02% sodium azide, and homogenized with a Tissumizer (Tekmar, Cincinnati, OH). Homogenates were centrifuged at 5000×*g* for 30 min at 4°C, and supernatants were saved for further analysis. The protein concentration of each supernatant was determined using a BCA Protein Assay (Pierce Biotechnology, Rockford, IL). The samples were analyzed immediately or stored at −80°C.

MMP-2/9 were detected by their capacity to degrade gelatin. Substrate gel electrophoresis (zymography) was carried out on a 7% polyacrylamide gel containing 1 mg/ml of gelatin (Sigma, St. Louis, MO), in the presence of sodium dodecyl sulfate (SDS). For each blood, liver or B16F10 tumor supernatant, 30 μg protein/lane (70 μg protein/lane for MDA-MB-435 tumor supernatant) was loaded under nondenaturing conditions and run at a constant voltage of 210 V for 5 h in a PROTEAN II Ready Gel System (Bio-Rad, Richmond, CA). Prestained molecular weight color standard (30 μl) and zymography standard containing MMP-2 and MMP-9 enzymes (25 ng for each) were included in each gel. Gels were washed twice in 2.5% Triton X-100 for 30 min and then incubated in 50 mM Tris–HCl buffer, pH 7.4, containing 0.15 mM NaCl, 0.02% sodium azide at 37°C for 18 h. Each gel was stained in 0.05% Coomassie blue R-250 and destained in 10% methanol–10% acetic acid. Gelatinolytic activity was detected as clear bands on a blue background on the stained gels. Zymography was performed at least twice for each sample.

2.11. Metabolism of ^{64}Cu-DOTA-CTT in B16F10 tumor-bearing mice

Mice bearing B16F10 tumor implants ($n=3$) were injected with 2 mCi of ^{64}Cu-DOTA-CTT in 100 μl of isotonic saline via the tail vein. The mice were anesthetized and sacrificed at 1 h postinjection. Blood was aspirated, and liver and tumor were harvested from the animals. Samples

Table 1
Inhibition of MMP-2 and MMP-9[a]

	EC_{50} (μM)		
	hMMP-2	mMMP-9	hMMP-9
CTT	13.2±1.6	11.0±2.5	9.6 (9.5–9.8)
Cu(II)-DOTA-CTT	8.7 (7.9–9.4)	18.2 (9.7–26.7)	8.6 (7.8–9.4)
STT	>1000[a]	104 (79–129)	ND
Cu(II)-DOTA-STT	>1000[b]	20.4 (14.3–26.4)	ND
Ilomastat (GM6001)	0.0004±0.0003	0.00013±0.00007	0.00012 (0.00005–0.00018)

ND=not determined.

[a] Each fluorescence activity measurement was made in triplicate. EC_{50} values were calculated by nonlinear regression for each activity curve. Data here represents the mean±S.D. for $n \geq 3$ activity curves or mean (range) for $n=2$.

[b] $n=1$.

were immediately rinsed with cold water to remove as much blood as possible, placed on ice and homogenized in 65:35 ethanol/ammonium acetate buffer (0.1 M, pH 5.5) using a Tissumizer for 2 min, followed by 30 s of sonication on a Sonifier 185 cell disruptor (Branson, Danbury, CT). Centrifugation (23,500×g) at 4°C for 30 min was performed to separate the insoluble protein and cellular debris. Size-exclusion HPLC was performed on 50 μl of each supernatant after direct injection. Fractions were collected in 60 s intervals and counted on a gamma counter. As a control for normalization of % activity in low molecular weight samples, ^{64}Cu-DOTA-CTT (500 μCi in 20 μl saline) was mixed with blood, liver or tumor homogenates (organ blank) ex vivo immediately before size exclusion HPLC analysis.

3. Statistical analysis

Data are expressed as mean±S.D. or mean (range) if $n=2$. Statistical analysis was performed using GraphPad Prism 4.0. Differences were considered statistically significant for $P<.05$.

4. Results

4.1. DOTA-CTT Synthesis

Although thalium trifluoroacetate is widely used to perform intramolecular disulfide cyclization of peptides on solid support, this strategy was not successful for the CTT peptides. Direct attachment of a cysteine amino acid residue needed for this reaction to the resin probably inhibits the reaction by steric effects. For this reason, disulfide cyclization of CTT peptides is conventionally performed in solution. However, we found that the desired compound can be isolated in 8% yield by first cyclizing the Fmoc-protected peptide on solid support, followed by Fmoc removal before adding DOTA. Although the desired compound was obtained by the method described above, product isolation required repeated HPLC purification steps, which is reflected in the low yield obtained.

4.2. Complexation chemistry

Cu(II)-DOTA-CTT and Cu(II)-DOTA-STT were analyzed by analytical reversed-phase HPLC (UV detection 214 nm) using conditions described in Materials and Methods and by ES-MS. Cu-64-DOTA-CTT and ^{64}Cu-DOTA-STT were prepared in ≥95% radiochemical purity as confirmed by radio-TLC or radio-RP-HPLC. Specific activities for both ^{64}Cu-labeled conjugates ranged from 450 to 1500 Ci/mmol (16,650 to 55,500 GBq/mmol).

4.3. Inhibition studies

Inhibition of MMP-2/9 by CTT was time-dependent (data not shown); mMMP-9 activity was reduced to <5% activity (50 μM CTT) after 2 h of preincubation of the enzyme and inhibitor. Significant inhibition was also observed for hMMP-2 and hMMP-9 at this time point. Therefore, 2 h of preincubation of enzyme and inhibitor was used for all inhibitory activity studies. Inhibition of MMP-2/9 by the control competitive inhibitor Ilomastat was not time-dependent.

Inhibition assays were performed for hMMP-9, mMMP-9 and hMMP-2 (Table 1). Human and mouse MMP-9 show 64% identity (BLASTp sequence alignment), so differences in inhibition by CTT could not be excluded. However, human and mouse MMP-2 show high homology (91% identity; zinc-dependent MMP domain: residues 122–214, 97% identity); thus, only the commercially available hMMP-2 was examined. Example enzyme activity curves, shown in Fig. 2, suggest that CTT is a partial inhibitor of hMMP-2 and hMMP-9 and a complete inhibitor of mMMP-9. Similarly, partial inhibition of hMMP-2 and hMMP-9 was observed for Cu(II)-DOTA-CTT (not shown). Poor curve fitting was observed using nonlinear regression for one-site competitive binding. Therefore, variable slope analysis was used to fit enzyme activity curves to calculate EC_{50} values for CTT, Cu(II)-DOTA-CTT, STT and

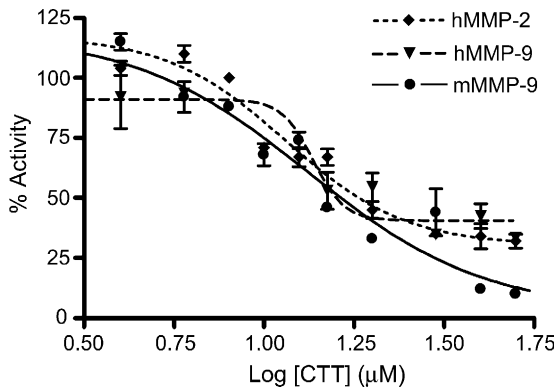

Fig. 2. Activity curves for hMMP-2, hMMP-9 and mMMP-9 in the presence of increasing concentrations of CTT for determination of EC_{50} values. Each data point ($n=3$) is normalized to control enzyme activity. Nonlinear regression was used to fit each curve.

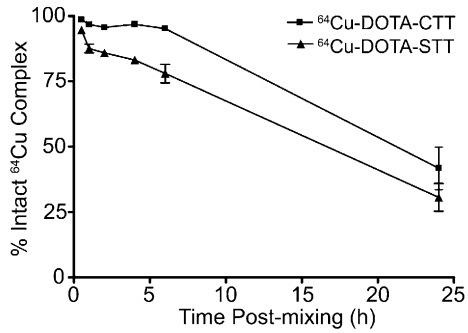

Fig. 3. Serum stability of ^{64}Cu-DOTA-CTT and ^{64}Cu-DOTA-STT. The % intact complex was monitored by radio-TLC at multiple time points ($n=4$).

Cu(II)-DOTA-STT (structures, Fig. 1). For partial inhibitors, the EC_{50} was determined as the concentration at which 50% of the response to that inhibitor was observed; for complete inhibitors, EC_{50} was equal to IC_{50}. The EC_{50} values determined for the control inhibitor Ilomastat (GM6001), a complete inhibitor, and CTT were in close agreement with literature values [20,35,41]. There was no statistical difference in the inhibitory activity of Cu(II)-DOTA-CTT and CTT for hMMP-9 or mMMP-9 (Table 1); the EC_{50} values for hMMP-2 were similar (4.5 μM difference). Thus, conjugation of CTT to the chelator DOTA does not significantly change the affinity of the ligand for MMP-2/9.

Cu-64-DOTA-D-Trp-CTT (CTT**HwGF**TLC) was initially proposed as a negative control peptide. A preliminary microPET imaging study using B16F10 tumor-bearing mice demonstrated equivalent tumor uptake of ^{64}Cu-DOTA-CTT and ^{64}Cu-DOTA-D-Trp-CTT. These data suggest that modification of CTT by introduction of D-Trp may not change peptide targeting. Therefore, the negative control peptide was redesigned to incorporate a scrambled active motif and replace Cys residues with Ser resulting in the linear peptide STT (STT**GHFW**TLS); linearization had previously been reported to reduce MMP-2 inhibitory activity 10-fold [20]. hMMP-2 was not inhibited by STT or Cu(II)-DOTA-STT (EC_{50} >1000 μM). The inhibitory activity of STT for mMMP-9 was 10-fold lower than for inhibition by CTT. However, Cu(II)-DOTA-STT inhibited mMMP-9 with similar affinity as Cu(II)-DOTA-CTT ($P=.85$). Thus, hMMP-2 inhibition may be more sensitive to changes in the HWGF active sequence or cyclic peptide structure than mMMP-9. Inhibition of hMMP-9 by STT and Cu(II)-DOTA-STT was not evaluated as no human tumors were to be used with this peptide.

4.4. In vitro stability

The serum stability of ^{64}Cu-DOTA-CTT and ^{64}Cu-DOTA-STT was evaluated. Radio-HPLC at 1 h postmixing revealed no change in retention time for ^{64}Cu-DOTA-CTT indicating intact peptide and complex. Similarly, radio-HPLC of ^{64}Cu-DOTA-STT (1 h) showed no change in retention time for complexed ^{64}Cu. Additional time points were examined using radio-TLC; from 0 to 6 h, there was no significant breakdown of ^{64}Cu-DOTA-CTT in serum (>95 % intact) (Fig. 3). However, the % intact ^{64}Cu complex was significantly reduced by 24 h (41.7±8.1%). The percentage of complexed ^{64}Cu for ^{64}Cu-DOTA-STT, as determined by radio-TLC, was lower at all time points, revealing reduced stability of ^{64}Cu-DOTA-STT in rat serum compared to ^{64}Cu-DOTA-CTT.

4.5. Detection of MMP-2/9 in B16F10 tumor-bearing mice

To determine the in vivo properties of ^{64}Cu-DOTA-CTT, this agent was first evaluated in normal, non-tumor-bearing mice. Cu-64-DOTA-CTT cleared slowly from the kidney (7.59±1.86 %ID/g at 1 h, 4.24±0.53 %ID/g at 24 h). No significant change in blood (0.792±0.21 %ID/g at 1 h, 0.59±0.23 %ID/g at 24 h) or liver (9.80±2.19 %ID/g at 1 h, 8.70±1.59 %ID/g at 24 h) uptake was observed over this period.

The biodistribution of ^{64}Cu-DOTA-CTT and ^{64}Cu-DOTA-STT in B16F10 tumor-bearing mice was evaluated (Table 2). Cu-64-DOTA-CTT showed tumor accumulation (2.44±0.26 % ID/g) 2 h postinjection in tumor-bearing mice. Copper-64-DOTA-CTT demonstrated higher uptake in every organ examined than did ^{64}Cu-DOTA-STT. The tumor/blood ratio was 2.12±0.70 for ^{64}Cu-DOTA-CTT and 1.82±0.68 for ^{64}Cu-DOTA-STT; this difference was not significant ($P=.56$).

Concurrent with biodistribution, a microPET imaging study was carried out to compare ^{64}Cu-DOTA-CTT and ^{64}Cu-DOTA-STT in the B16F10 tumor model (12 days postimplantation) (Fig. 4). Mice receiving ^{64}Cu-DOTA-CTT had visible tumor uptake at all time points (1, 4 and 24 h) ($n=2$). In contrast, tumor uptake was not visible or very low in the mice receiving ^{64}Cu-DOTA-STT ($n=2$).

Zymography was performed on tumor, blood and liver extracts to examine MMP-2/9 expression. Various concentrations of purified MMP-2 and MMP-9 were examined by zymography (data not shown) to determine that the limit for detection of either gelatinase was 5–10 ng. This was used to calculate the minimal detectable limit [(5–10 ng/enzyme molecular weight)/mass protein loaded] for MMP-2 (2300–4600 fmol/mg protein) and MMP-9 (1800–3600 fmol/mg protein) zymography of tissue samples. Both MMP-9 and

Table 2
Biodistribution of ^{64}Cu-DOTA-CTT and ^{64}Cu-DOTA-STT in B16F10 tumor-bearing mice at 2 h postinjection at 13 days posttumor implantation ($n=5$)

Organs	% ID/g	
	^{64}Cu-DOTA-CTT	^{64}Cu-DOTA-STT
Blood	1.15±0.36	0.50±0.18
Lung	5.21±0.64	1.78±0.38
Liver	11.74±2.08	5.37±1.17
Spleen	1.50±0.58	0.64±0.21
Kidney	12.51±3.04	5.46±1.34
Bone	1.08±0.41	0.59±0.28
Tumor	2.44±0.26	0.91±0.10

Data are presented as %ID/g±S.D.

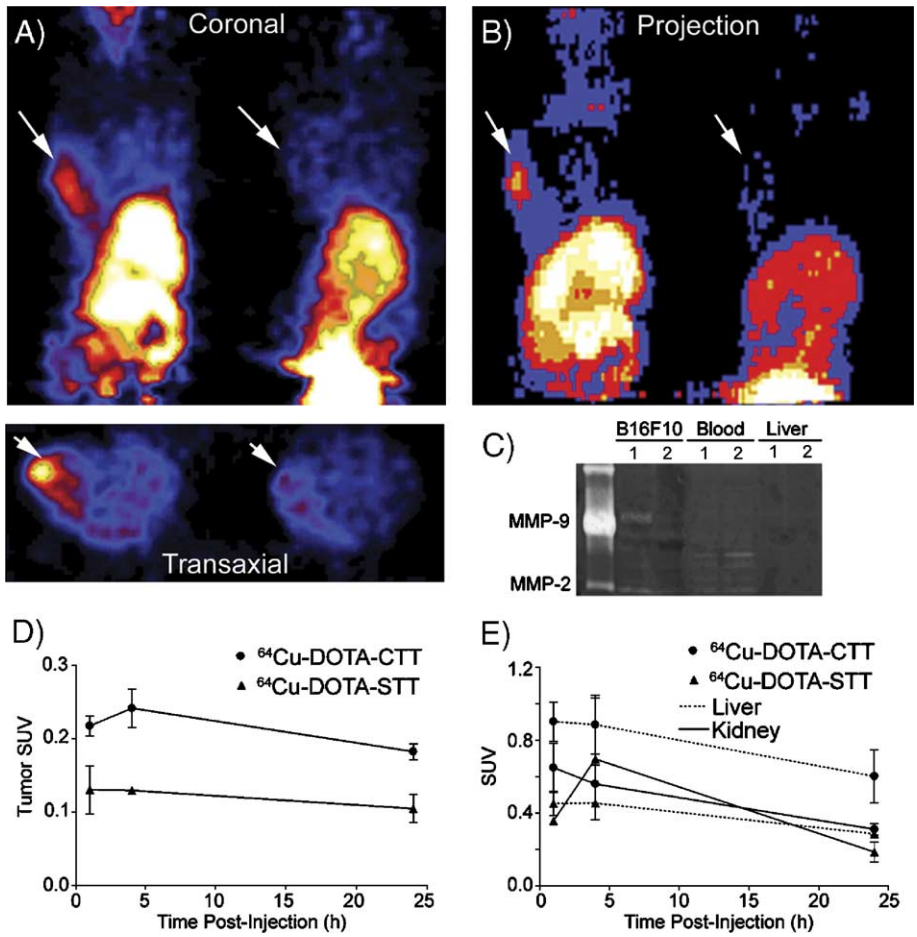

Fig. 4. Detection of MMP-2/9 overexpression in B16F10 tumors. Anesthetized (1–2% isoflurane) C57BL/6 mice bearing B16F10 tumors (12 days post-implantation) were microPET imaged (10-min scan) following injection of ^{64}Cu-DOTA-CTT (left, 205 μCi, 1.5 μg) and ^{64}Cu-DOTA-STT (right, 173 μCi, 0.36 μg). Coronal and transaxial slices (A) are shown as well as a maximum intensity projection (B) to permit viewing of the whole-body image. Tumors are indicated by arrows. Zymography (30 μg protein/well) was performed on tissue samples from two tumor-bearing mice to determine relative levels of MMP-2 and MMP-9 in target and nontarget organs (C). Tissue time–activity curves of ^{64}Cu-DOTA-CTT and ^{64}Cu-DOTA-STT were generated for B16F10 tumor (D) and liver and kidney (E) ($n=2$).

MMP-2 were detectable in B16F10 tumor extracts and, to a lesser extent, in blood (Fig. 4). No gelatinase activity was detectable in mouse liver.

Standard uptake values for tumor, kidney and liver were calculated by measuring the radioactivity in each organ ROI from the microPET images (Fig. 4D,E). Tumor uptake of ^{64}Cu-DOTA-CTT is about twofold greater than that of ^{64}Cu-DOTA-STT at all time points; this is similar to the fold difference observed in the biodistribution study. However, higher liver and kidney uptake were also observed in tumor-bearing mice receiving ^{64}Cu-DOTA-CTT compared to those receiving ^{64}Cu-DOTA-STT.

4.6. Imaging MMP-2/9 in MDA-MB-435 tumor-bearing mice

Imaging data demonstrating better B16F10 tumor uptake for ^{64}Cu-DOTA-CTT than for the negative control ^{64}Cu-DOTA-STT were encouraging despite limited differences between these compounds by biodistribution. Therefore, a second tumor model, MDA-MB-435, was investigated to follow changes in gelatinase expression over time. Female *nu*/*nu* mice were orthotopically implanted with 1×10^5 MDA-MB-435 cells for microPET imaging between 7 and 13 weeks postimplantation. Extra mice were implanted as only 50–75% of mice were expected to develop tumors based on experience in this laboratory. Therefore, some extra tumor-bearing mice were sacrificed without microPET imaging.

Example microPET images at 1 h postinjection of ^{64}Cu-DOTA-CTT in MDA-MB-435 tumor-bearing mice are shown in Fig. 5. Tumor uptake was clearly visible in one mouse imaged at 7 weeks postimplantation (left) (1 h tumor SUV$=0.525\pm0.092$). Although tumor uptake was elevated in the region of the tumor for a second mouse (right) imaged at 7 weeks (1 h tumor SUV$=0.408\pm0.028$), this uptake was diffuse across the entire chest with highest uptake apparent in the left mammary fat pad. Upon dissection, no tumor was visible in the left mammary fat pad. In addition, biodistribution of this mouse further revealed elevated uptake in lung and heart relative to the first mouse (data not shown).

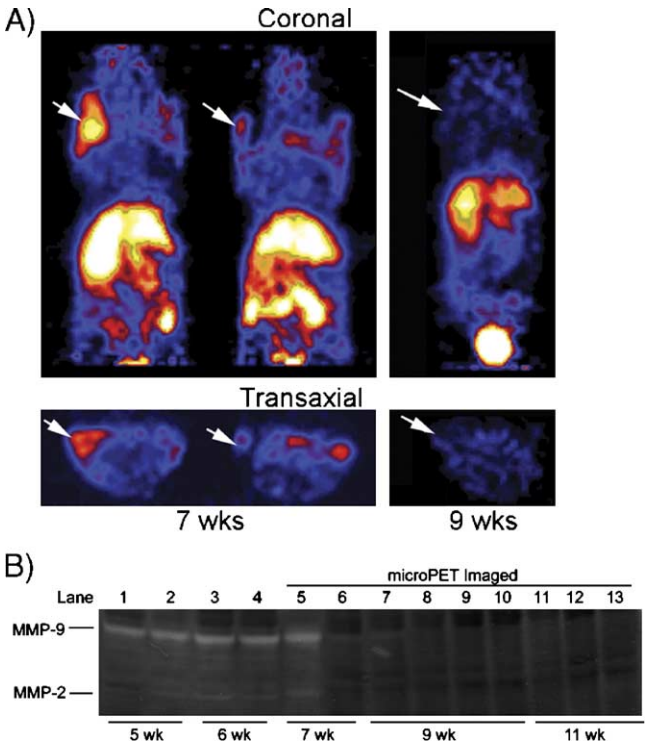

Fig. 5. MicroPET imaging with ^{64}Cu-DOTA-CTT was performed on anesthetized (1–2% isoflurane) MDA-MB-435 tumor-bearing mice. MicroPET images (10-min scan) are shown at 7 weeks (left=207 μCi, 1.5 μCi; center=209 μCi, 1.5 μg) and 9 weeks (right=159 μCi, 2.4 μg) post-implantation (1 h post-injection) as coronal and transaxial slices (A). Tumor masses were as follows: left=44 mg, center=326 mg, right=765 mg. Tumors are indicated by arrows. Zymography of tumor extracts (70 μg protein/well) for mice sacrificed 5–11 weeks post-implantation is shown (B). Time postimplantation is indicated below the gels. Lanes 5–13 contain tumor extracts from mice that were microPET imaged.

Thus, this uptake could not be solely attributed to the tumor. Tumor uptake was not evident in the 9 weeks post-implantation mouse shown (right) (1 h tumor SUV=0.102±0.005) or in the remaining nine tumor-bearing mice that were imaged and sacrificed between 9 and 13 weeks postimplantation (1 h tumor SUV=0.083±0.026). As tumors did not appear to be detectable at later times postimplantation, microPET imaging of tumors greater than 13 weeks was not carried out.

Zymography results for MDA-MB-435 tumors from 5 to 11 weeks postimplantation are shown in Fig. 5B. Zymography detection limits for MDA-MB-435 tumor samples (70 μg protein/well) were calculated to be 990–1990 fmol/mg protein for MMP-2 and 770–1560 fmol/mg protein for MMP-9 based on the methods described above. In this study, MMP-9 activity bands were clearly visible (Lanes 1–4) for tumors from mice sacrificed at 5 and 6 weeks postimplantation. However, these mice were not imaged prior to sacrifice. In addition, MMP-2 was detectable (very faint, Lane 1; faint, Lanes 2–4) in these mice. Both MMP-2 and MMP-9 activity bands were visible for one mouse imaged at 7 weeks (Lane 5); this corresponded to the single mouse for which the tumor was clearly visible by microPET imaging (Fig. 5A, left). MMP-2 and MMP-9 activity bands were not detectable in the second mouse imaged at 7 weeks (Lane 6) which had shown diffuse uptake including the tumor region by microPET (Fig. 5A, center). No MMP activity was detectable in tumors after 7 weeks postimplantation; these corresponded to tumors that were not visible by microPET with ^{64}Cu-DOTA-CTT. MMP activity was blocked by incubation of the gels in development buffer containing 20 mM EDTA (data not shown).

As MMP-2/9 expression appeared to occur early after implantation, a second set of mice were implanted with MDA-MB-345 tumors for microPET imaging. Twelve tumor-bearing mice (6–9 weeks postimplantation) were imaged at 1 h post-injection of ^{64}Cu-DOTA-CTT. No tumors were visible by microPET in any of these mice (data not shown). In addition, MMP-2/9 was undetectable by zymography (data not shown). Thus, expression of MMP-2/9 by MDA-MB-435 tumors was not consistent among the 25 tumors evaluated.

4.7. In vivo metabolism

Significant accumulation of radioactivity in the blood and liver was observed for all ^{64}Cu-DOTA-CTT-treated animals. Therefore, the in vivo metabolism of ^{64}Cu-DOTA-CTT was examined in blood, liver and tumor homogenates from B16F10 tumor-bearing mice (1 h post-injection) using size-exclusion HPLC. Late eluting, low molecular weight (<5000 Da) fractions were defined using organ blank experiments as control. Here, ^{64}Cu-DOTA-CTT was added ex vivo to blood, liver or tumor homogenates from non-injected mice immediately before analysis by size-exclusion HPLC; the percentage of activity in low molecular weight fractions was used as a normalization factor. At 1 h PI, the normalized protein bound fractions (>5000 Da) were 85.9±7.3% for blood, 94.7±1.5% for liver and 89.5±1.6% for tumor (n=3). The majority of protein-bound ^{64}Cu in liver extract had an elution time corresponding to a molecular weight of ~34 kDa, suggesting superoxide dismutase (SOD) is the primary ^{64}Cu-labeled protein in mouse blood and liver as was previously demonstrated for ^{64}Cu-DOTA [42]. However, these fractions may also have include ^{64}Cu-DOTA-CTT that was bound to proteins in vivo. The remaining ^{64}Cu eluted at later retention times, representing <5000 Da intact, unbound complex. Thus, ^{64}Cu-DOTA-CTT appears to be less stable in vivo than was predicted by in vitro serum stability at 1 h (>95% intact complex).

5. Discussion

The cyclic peptide CTT was identified by Koivunen et al. [20] as a selective gelatinase inhibitor that inhibits both the pro and active forms of the enzyme. Here we conjugated CTT to the chelator DOTA for radiolabeling with ^{64}Cu for microPET imaging of MMP-2/9 in tumors. Attachment of

Cu(II)-DOTA to CTT did not significantly affect the affinity of the peptide for gelatinases (Table 1). In contrast, the mMMP-9 EC_{50} for STT (negative control) was 10-fold higher than for CTT, but there was no difference in mMMP-9 EC_{50} value between Cu(II)-DOTA-STT and Cu(II)-DOTA-CTT. MMP-2 was not inhibited (EC_{50} >1000 μM) by either STT or Cu(II)-DOTA-STT. Thus, hMMP-2 may be more sensitive to changes in the active HWGF motif of CTT, and/or cyclization of the peptide, while other factors may play a greater role in mMMP-9 inhibition. Compared to nonpeptide competitive MMP inhibitors such as ilomastat, ^{64}Cu-DOTA-CTT is a relatively low-affinity ligand [35]. Higher affinity is generally desirable to increase specific target organ uptake in vivo.

To better understand whether ~10 μM affinity of ^{64}Cu-DOTA-CTT is sufficient for detection of gelatinases in tumors, B_{max}/K_d was estimated. The concentration of mMMP-9 in B16F10 tumors can be converted into a B_{max} value by assuming that 1 fmol receptor/mg protein=0.1 nM; this approximation can be used for estimating receptor concentration [43]. K_i for mMMP-9 was calculated using the equation: $K_d=K_i=IC_{50}/[1+(\text{substrate})/K_m]$. For mMMP-9, this yielded a B_{max}/K_d ratio range of 51–103 in B16F10 tumors. It has been previously reported that a B_{max}/K_d ratio =10 is sufficient for planar imaging for radiotracers with nanomolar affinities [44]. These data are encouraging. However, if any higher affinity ligands for MMP-2/9 are present in the tumor, these ligands would compete with ^{64}Cu-DOTA-CTT for target binding. In addition, because low-affinity ligands typically have high off-rates, it is unclear if enough specifically bound ^{64}Cu-DOTA-CTT will remain in the tumor for detection by PET after allowing sufficient time for clearance of nonspecifically bound radiotracer.

It was noted that CTT and Cu(II)-DOTA-CTT demonstrated only partial inhibition of hMMP-2 and hMMP-9 even at concentrations 4 orders of magnitude above the concentration of the enzyme. Similar partial inhibition of MMP-2 by CTT was previously observed using a different assay system when this peptide was reported by Koivunen et al. [20] as a selective gelatinase inhibitor. EC_{50} curves for these inhibitors were best fit using variable-slope nonlinear regression. Although we did not investigate the mechanism of inhibition, this may suggest that multiple CTT peptides must bind to the enzyme with possible cooperativity to induce inhibition.

The murine melanoma B16F10, which overexpresses gelatinases in vivo, demonstrated higher than background uptake of ^{64}Cu-DOTA-CTT in microPET imaging studies (Fig. 4). Tumor radioactivity was significantly lower in mice imaged with ^{64}Cu-DOTA-STT. However, biodistribution revealed no significant difference in tumor/blood ratio between ^{64}Cu-DOTA-CTT and ^{64}Cu-DOTA-STT. There are several problems associated with ^{64}Cu-DOTA-STT as a negative control; these include reduced in vivo stability of linear peptides and similar binding affinity to one of the two targeted gelatinases (mMMP-9) compared to Cu(II)-DOTA-CTT. Thus, specific uptake of ^{64}Cu-DOTA-CTT by gelatinase-expressing tumors was not clearly demonstrated in the B16F10 melanoma model.

MMP-2/9 expression imaging was also examined in MDA-MB-435 human breast cancer tumors in mice. In our initial study, uptake of ^{64}Cu-DOTA-CTT was clearly localized to tumor in a single mouse imaged at 7 weeks postimplantation but not in the remaining 11 mice imaged at 7–13 weeks postimplantation. Zymography results for these mice supported selective uptake by MMP-2/9-expressing tumors; MMP-2 and MMP-9 activity was detected only in the tumor that was visualized by microPET (Fig. 5, Lane 5), but not in the remaining imaged tumors that showed no uptake of ^{64}Cu-DOTA-CTT. However, the small sample size of positive, imaged tumors and early time points of MMP-2/9 expressing tumors necessitated imaging of a second implantation group (6–9 weeks postimplantation). No tumors were visualized by microPET of 12 MDA-MB-435 tumor-bearing mice, and no gelatinase expression was detectable in these tumor extracts. The lack of MMP-2/9 expression by most MDA-MB-435 tumors in vivo was not expected, as MDA-MB-435 cells have been shown in several studies to express both MMP-2 and MMP-9 proteins in vitro [45,46], and MDA-MB-435 tumor growth has been shown to be inhibited by the MMP-2 and MMP-9 selective inhibitor CTT [20]. However, a conflicting report by Tester et al. [47] showed that MMP-2 and MMP-9 mRNA were not present in MDA-MB-435 cells in culture. Thus, our results in MDA-MB-435 tumor-bearing mice are consistent with targeted imaging of MMP-2/9. However, poor reproducibility of gelatinase expression by MDA-MB-435 tumors renders this model inutile for validation of new gelatinase-targeting imaging technologies.

The CTT peptide is highly lipophilic [21,48]. Lipophilic compounds are expected to bind nonspecifically to albumin in the blood. The leaky vasculature in tumors causes albumin to accumulate; this property has been exploited in the MRI field for assessment of tumor microvascular permeability [49]. Thus, some tumor uptake of ^{64}Cu-DOTA-CTT may be due to nonspecific accumulation of ^{64}Cu-DOTA-CTT-albumin. However, it is unlikely that this mechanism plays a major role in tumor uptake since so few MDA-MB-435 tumors were visualized with this radiotracer.

Both biodistribution and microPET imaging demonstrated high liver and blood uptake of ^{64}Cu-DOTA-CTT despite lack of gelatinase expression in these organs, as demonstrated by zymography (Fig. 4). Lipophilic compounds like CTT have significant clearance through the hepatobiliary system and high liver uptake. CTT has been shown to bind to liposomes [48]; Kuhnast et al. [21] suggested that this property could lead CTT to bind to blood cell membranes, thus leading to high blood uptake. As stated above, blood uptake is also likely increased by binding of ^{64}Cu-DOTA-CTT to albumin.

In addition, the poor clearance properties observed for ^{64}Cu-DOTA-CTT can be partially explained by the use of DOTA as chelator. DOTA is frequently employed as a bifunctional chelator because it is compatible with a variety of metals including Cu, In, Ga, Y and Lu. However, studies in our laboratory, completed after the inception of this project, clearly demonstrate that ^{64}Cu-DOTA (1 h; blood: 39% protein bound; liver: 87% protein bound) is significantly less stable in vivo than other Cu(II)-tetraazamacrocyclic complexes such as ^{64}Cu-TETA (1,4,8,11-tetraazacyclotetradecane-1,4,8,11-tetraacetic acid) (1 h; blood: 8% protein bound; liver: 32% protein bound) and ^{64}Cu-CB-TE2A (4,11-bis(carboxymethyl)-1,4,8,11-tetraazabicyclo[6.6.2]hexadecane) (1 h; blood: 15% protein bound; liver: 14% protein bound) due to increased transchelation of Cu(II) to proteins [42]; this has been shown to result in high background radioactivity uptake [42,50]. These data did not predict the high degree of ^{64}Cu-DOTA-CTT instability in blood (1 h: 85.9±7.3% protein bound) observed in this study. This discrepancy suggests that at least some fraction of protein-bound radioactivity was due to protein-bound intact complex. Still, use of a different ^{64}Cu chelate or of another, more stable DOTA–radiometal complex may improve tumor/nontarget ratios.

In this study, we were unable to demonstrate specificity of tumor uptake by ^{64}Cu-DOTA-CTT due to poor in vivo stability of the complex and low ligand binding affinity. CTT was identified by phage display to be a specific gelatinase inhibitor [20]. In that system, each phage displays multiple copies of the peptide. Peptide affinity for gelatinases may therefore have been enhanced in vivo due to a multivalency effect. Presentation of the peptide on the phage surface may have also reduced proteolytic degradation by making the peptide less accessible, thereby increasing the in vivo stability. Thus, ^{64}Cu-DOTA-CTT is not an optimal PET imaging agent, although more stable, higher affinity derivatives may still be useful for selective imaging of gelatinases in tumors.

Acknowledgments

The authors acknowledge Todd A. Perkins and Deborah Sultan for production of ^{64}Cu; Susan Adams, Laura Meyer, Chris Sherman, Lynne A. Jones, Nicole Fettig, John Engelbach and Lori Strong for their excellent technical assistance; and Jerrel Rutlin for help in microPET data analysis. This research was supported by NCI grant R21 CA098698. The production of ^{64}Cu at Washington University School of Medicine is supported by the NCI grant R24 CA86307. Small animal imaging at Washington University School of Medicine is supported by the NIH grant 5 R24 CA83060. J.E.S. was supported by the NIH Medical Scientist Training Program Grant T32 GM07200-2, the Department of Energy Training Grant DE F0101 NE23051 and the Department of Defense Breast Cancer Research Program Grant W81XWH-04-1-0396.

References

[1] Egeblad M, Werb Z. New functions for the matrix metalloproteinases in cancer progression. Nat Rev Cancer 2002;2:163–76.
[2] Cotran RS, Kumar V, Collins T. Robbins pathologic basis of disease. 6th ed. Philadelphia: W.B. Saunders; 1999.
[3] Matrisian LM. Metalloproteinases and their inhibitors in tissue remodeling. Trends Genet 1990;6:121–5.
[4] Woessner JF. Matrix metalloproteinases and their inhibitors in connective tissue remodeling. FASEB J 1990;5:2145–54.
[5] Stetler-Stevenson WG. Type IV collagenases in tumor invasion and metastasis. Cancer Metastasis Rev 1990;9:289–303.
[6] Tryggvason K, Hoyhta M, Salo T. Proteolytic degradation of extracellular matrix in tumor invasion. Biochim Biophys Acta 1987;907:191–217.
[7] Tryggvason K. Type-IV collagenase in invasive tumors. Breast Cancer Res Treat 1993;24:209–18.
[8] Itoh T. Reduced angiogenesis and tumor progression in gelatinase—A deficient mice. Cancer Res 1998;58:1048–51.
[9] Coussens LM, Tinkle CL, Hanahan D, Werb Z. MMP-9 supplied by bone marrow-derived cells contributes to skin carcinogenesis. Cell 2000;103:481–90.
[10] Vilinen P, Kahari V-M. Matrix metalloproteinases in cancer: prognostic markers and therapeutic targets. Int J Cancer 2002;99:157–66.
[11] Talvensaari-Mattila A, Paakko P, Turpeenniemi-Hujanen T. Matrix metalloproteinase-2 (MMP-2) is associated with survival in breast carcinomas. Br J Cancer 2003;89:1270–5.
[12] Talvensaari-Mattila A, Paakko P, Turpeenniemi-Hujanen T. MMP-2 positivity and age less than 40 years increases the risk for recurrence in premenopausal patients with node-positive breast carcinoma. Breast Cancer Res Treat 1999;58:287–93.
[13] Talvensaari-Mattila A, Paakko P, Blanco-Sequeiros G, Turpeenniemi-Hujanen T. Matrix metalloproteinase-2 (MMP-2) is associated with the risk for a relapse in postmenopausal patients with node-positive breast carcinoma treated with antiestrogen adjuvant therapy. Breast Cancer Res Treat 2001;65:55–61.
[14] Bremer C, Tung C-H, Weissleder R. In vivo molecular target assessment of matrix metalloproteinase activity. Nat Med 2001;7:743–8.
[15] Zheng Q-H, Fei X, DeGrado TR, Wang J-Q, Lee Stone K, Martinez TD, et al. Synthesis, biodistribution and micro-PET imaging of a potential cancer biomarker carbon-11 labeled MMP inhibitor (2*R*)-2-[[4-(6-fluorohex-1-ynyl)phenyl]sulfonylamino]-3-methylbutyric acid [^{11}C]methyl ester. Nucl Med Biol 2003;30:753–60.
[16] Kulasegaram R, Giersing B, Page CJ, Blower PJ, Williamson RA, Peters BS, et al. In vivo evaluation of In-111-DTPA-N-TIMP-2 in Kaposi's sarcoma associated with HIV infection. Eur J Nucl Med 2001;28:756–61.
[17] Zheng Q-H, Fei X, Liu Z, Wang J-Q, Stone KL, Martinez TD, et al. Comparative studies of potential cancer biomarkers carbon-11 labeled MMP inhibitors (*S*)-2-(4′-[^{11}C]methoxybiphenyl-4-sulfonylamino)-3-methoxyphenyl)sulfonyl]benzylamino]-3-methylbutanamide. Nucl Med Biol 2004;31:77–85.
[18] Oltenfreiter R, Staelens L, Lejeune A, Dumont F, Frankenne F, Foidart JM, et al. New radioiodinated carboxylic and hydroxamic matrix metalloproteinase inhibitor tracers as potential tumor imaging agents. Nucl Med Biol 2004;31:459–68.
[19] Furumoto S, Takashima K, Kubota K, Ido T, Iwata R, Fukuda H. Tumor detection using ^{18}F-labeled matrix metalloproteinase-2 inhibitor. Nucl Med Biol 2003;30:119–25.
[20] Koivunen E, Arap W, Valtanen H, Rainisalo A, Medina OP, Heikkila P, et al. Tumor targeting with a selective gelatinase inhibitor. Nat Biotechnol 1999;17:768–74.
[21] Kuhnast B, Bodenstein C, Haubner R, Wester HJ, Senekowitsch-Schmidtke R, Schwaiger M, et al. Targeting of gelatinase activity with a radiolabeled cyclic HWGF peptide. Nucl Med Biol 2004;31:337–44.

[22] Medina OP, Kairemo K, Valtanen H, Kangasniem A, Kaukenen S, Ahonen I, et al. Radionuclide imaging of tumor xenografts in mice using a gelatinase-targeting peptide. Anticancer Res 2005;25:33–42.
[23] McCarthy DW, Shefer RE, Klinkowstein RE, Bass LA, Margeneau WH, Cutler CS, et al. Efficient production of high specific activity Cu-64 using a biomedical cyclotron. Nucl Med Biol 1997;24:35–43.
[24] Lewis JS, Lewis MR, Cutler PD, Srinivasan A, Schmidt MA, Schwartz SW, et al. Radiotherapy and dosimetry of ^{64}Cu-TETA-Tyr^3-Octreotate in a somatostatin receptor-positive, tumor-bearing rat model. Clin Cancer Res 1999;5:3608–16.
[25] Connett JM, Anderson CJ, Guo L-W, Schwartz SW, Zinn KR, Rogers BE, et al. Radioimmunotherapy with a Cu-64 labeled monoclonal antibody: a comparison with Cu-67. Proc Natl Acad Sci U S A 1996; 93:6814–8.
[26] Lewis MR, Wang M, Axworthy DB, Theodore LJ, Mallet RW, Fritzberg AR, et al. In vivo evaluation of pretargeted Cu-64 for tumor imaging and therapy. J Nucl Med 2003;44:1284–92.
[27] McCarthy DW, Shefer RE, Klinkowstein RE, Bass LA, Margenau WH, Cutler CS, et al. The efficient production of high specific activity Cu-64 using a biomedical cyclotron. Nucl Med Biol 1997;24:35–43.
[28] Atherton E, Sheppard RC. Solid phase peptide synthesis: a practical approach. Oxford (England): Oxford Univ. Press; 1989.
[29] Achilefu S, Jimenez HN, Dorshow RB, Bugaj JE, Webb EG, Wilhelm RR, et al. Synthesis, in vitro receptor binding, and in vivo evaluation of fluorescein and carbocyanine peptide-based optical contrast agents. J Med Chem 2002;45:2003–15.
[30] Achilefu S, Dorshow RB, Bugaj JE, Rajagopalan R. Novel receptor-targeted fluorescent contrast agents for in vivo tumor imaging. Invest Radiol 2000;35:479–85.
[31] Anderson CJ, Pajeau TS, Edwards WB, Sherman ELC, Rogers BE, Welch MJ. In vitro and in vivo evaluation of copper-64-labeled octreotide conjugates. J Nucl Med 1995;36:2315–25.
[32] Beekman B, Drijfhout JW, Bloemhoff W, Ronday HK, Tak PP, Koppele JM. Convenient fluorometric assay for matrix metalloproteinase activity and its application in biological media. FEBS Lett 1996;390:221–5.
[33] Bickett DM, Green MD, Berman J, Dezube M, Howe AS, Brown PJ, et al. A high throughput fluorogenic substrate for interstitial collagenase (MMP-1) and gelatinase (MMP-9). Anal Biochem 1993; 212:58–64.
[34] Medina OP, Soderlund T, Laakkonen LJ, Tuominen EKJ, Koivunen K, Kinnunen PKJ. Binding of novel peptide inhibitors of type IV collagenases to phospholipid membranes and use in liposome targeting to tumor cells in vitro. Cancer Res 2001;61:3978–85.
[35] Galardy RE, Cassabonne ME, Giese C, Gilbert JH, Lapierre F, Lopez H, et al. Low molecular weight inhibitors in corneal ulceration. Ann N Y Acad Sci 1994;732:315–23.
[36] Bakewell SJ, Nestor P, Prasad S, Tomasson MH, Dowland N, Mehrotra M, et al. Platelet and osteoclast beta 3 integrins are critical for bone metastasis. Proc Natl Acad Sci U S A 2003;100:14205–10.
[37] Price JE, Polyzos A, Zhang RD, Daniels LM. Tumorigenicity and metastasis of human breast carcinoma cell lines in nude mice. Cancer Res 1990;20:717–21.
[38] Cherry SR, Shao Y, Silverman RW, Meadors K, Siegel S, Chatziioannou A, et al. MicroPET: a high resolution PET scanner for imaging small animals. IEEE Trans Nucl Sci 1997;44: 1161–6.
[39] Knoess C, Siegel S, Smith A, Newport D, Richerzhagen N, Winkeler A, et al. Performance evaluation of the microPET R4 PET scanner for rodents. Eur J Nucl Med Mol Imaging 2003;30:737–47.
[40] Gonzalez-Avila G, Ituria C, Vadillo-Ortega F, Ovalle C, Montano M. Changes in matrix metalloproteinases during the evolution of interstitial renal fibrosis in a rat experimental model. Pathobiology 1998;66:196–204.
[41] Galardy RE, Cassabonne ME, Giese C, Gilbert JH, Lapierre F, Lopez H, et al. Low molecular weight inhibitors in corneal ulceration. Ann N Y Acad Sci 1994;732:315–23.
[42] Boswell CA, Sun X, Niu W, Weisman GR, Wong EH, Rheingold AL, et al. Comparative in vivo stability of copper-64-labeled cross-bridged and conventional tetraazamacrocyclic complexes. J Med Chem 2004;47:1465–74.
[43] Eckelman W. Developing a successful imaging probe: an overview: Society of Nuclear Medicine 52nd Annual Meeting, Toronto, Canada, 2005. http://interactive.snm.org/index.cfm?PageID=3902&RPID=3902&A=11&B=469.
[44] Eckelman W. The application of receptor theory to receptor-binding and enzyme-binding oncologic radiopharmaceuticals. Nucl Med Biol 1994;21:759–69.
[45] Bachmeier BE, Nerlich AG, Lichtinghagen R, Sommerhoff CP. Matrix metalloproteinases (MMPs) in breast cancer cell lines of different tumorigenicity. Anticancer Res 2001;21:3821–8.
[46] Rolli M, Fransvea E, Pilch J, Saven A, Felding-Habermann B. Activated integrin alpha v beta 3 cooperates with metalloproteinase MMP-9 in regulating migration of metastatic breast cancer cells. Proc Natl Acad Sci U S A 2003;100:9482–7.
[47] Tester AM, Waltham M, Oh S-J, Bae S-N, Bills MM, Walker EC, et al. Pro-matrix metalloproteinase-2 transfection increases orthotopic primary growth and experimental metastasis of MDA-MB-231 human breast cancer cells in nude mice. Cancer Res 2004;64: 652–8.
[48] Medina OP, Soderlund T, Laakkonen LJ, Tuominen EKJ, Koivunen E, Kinnunen PKJ. Binding of novel peptide inhibitors of type IV collagenases to phospholipid membranes and use in liposome targeting to tumor cells in vitro. Cancer Res 2001;61:3978–85.
[49] Brasch R, Turetschek K. MRI characterization of tumors and grading angiogenesis using macromolecular contrast media: status report. Eur J Radiol 2000;34:148–55.
[50] Sun X, Wuest M, Weisman GR, Wong EH, Reed DP, Boswell CA, et al. Radiolabeling and in vivo behavior of copper-64-labeled cross-bridged cyclam ligands. J Med Chem 2002;45:469–77.